Chinese Journal of
POLYMER SCIENCE

RESEARCH ARTICLE

https://doi.org/10.1007/s10118-024-3125-5
Chinese J. Polym. Sci.

Improving Thermal-oxidative Aging Resistance of Styrene-butadiene Rubber by Antioxidant Loaded Silica Aerogel

Xue-Fei Ping[a], Yu Wang[a], Lu Liu[a], Fu-Yong Liu[a,b*], Hong-Wei He[a], Pi Wang[a], Wen-Wen Yu[a,b], and Qiang Zheng[a,c*]

[a] *College of Materials Science and Engineering, Taiyuan University of Technology, Taiyuan 030024, China*
[b] *Shanxi-Zheda Institute of Advanced Materials and Chemical Engineering, Taiyuan 030032, China*
[c] *Key Laboratory of Macromolecular Synthesis and Functionalization, Department of Polymer Science and Engineering, Zhejiang University, Hangzhou 310058, China*

Electronic Supplementary Information

Abstract The antioxidant *N*-isopropyl-*N*'-phenyl-*p*-phenylenediamine (4010NA) was dissolved in ethanol and impregnated into silica aerogel (SAG) *via* vacuum-pressure cycles, yielding composite particles (A-N) with enhanced sustained-release and reinforcing capabilities. The effect of A-N on the mechanical properties and thermal-oxidative aging resistance of styrene-butadiene rubber (SBR) vulcanizates was investigated. TGA and BET assessments indicated that the loading efficiency of 4010NA in SAG reached 14.26% within ethanol's solubility limit. Incorporating A-N into SBR vulcanizates significantly elevated tensile strength by 17.5% and elongation at break by 41.9% over those with fumed silica and free 4010NA. Furthermore, A-N notably enhanced the thermal-oxidative aging resistance of SBR. After aging for 96 h at 100 °C, the tensile strength and elongation at break of SBR with A-N sustained 70.09% and 58.61% of their initial values, respectively, with the retention rate of elongation at break being 62.8% higher than that of SBR with fumed silica and free antioxidant. The study revealed that A-N composite particles significantly inhibited the crosslinking in SBR's molecular chains, reducing hardening and embrittlement during later thermal-oxidative aging stages.

Keywords Styrene-butadiene rubber; Silica aerogel; Loading modification; Thermal-oxidative aging

Citation: Ping, X. F.; Wang, Y.; Liu, L.; Liu, F. Y.; He, H. W.; Wang, P.; Yu, W. W.; Zheng, Q. Improving thermal-oxidative aging resistance of styrene-butadiene rubber by antioxidant loaded silica aerogel. *Chinese J. Polym. Sci.* https://doi.org/10.1007/s10118-024-3125-5

INTRODUCTION

Rubber, due to its outstanding elasticity and insulating characteristics, is acknowledged as a strategic material globally.[1,2] However, diene rubbers, particularly those containing double bonds, are highly susceptible to thermal-oxidative reactions under heat and oxygen exposure.[3,4] This results in a significant deterioration in its appearance, hardness, and mechanical properties, leading to a considerable reduction in its lifespan.[5,6]

The most prevalent method of preventing thermal-oxidative aging in rubber involves the addition of chemical antioxidants. These antioxidants react with active substances like oxygen and ozone, effectively inhibiting rubber aging. That's why maintaining a continuous supply of antioxidants throughout the service period of rubber materials is crucial in extending their service life.[7,8] However, an excessive addition of antioxidants can lead to their migration to the rubber surface, a phenomenon known as "blooming". This can decrease aging resistance, significantly diminish the rubber materials' mechanical properties, and result in environmental pollution.[9,10] Therefore, the proportion of antioxidants added to rubber materials is usually limited to about 1 wt%, meaning that thermal-oxidative aging resistance remains relatively constrained.[11] The challenge currently facing the rubber industry is how to increase the dose of antioxidants in rubber vulcanizates without causing their migration to the surface.

Chemical grafting of antioxidant to the surface of filler,[12–14] preparation of new reactive antioxidant[15] and macromolecular antioxidant[16,17] are very effective means to prevent the migration of antioxidant, which have achieved good results in improving thermal-oxidative aging resistance of rubber. However, their preparation method are complex and difficult to achieve large-scale industrialization. The straightforward and efficient process of physically loading antioxidants onto the carrier is gradually favored by all parties. A variety of inorganic carriers have been used to physically support different antioxidants to prepare composite antioxidants, including natural halloysite (HNTs-RD)[18] and synthetic mesoporous silica nanorods (MSN-SH-4020),[11,19] carbon nanotubes (CNT-4020),[20] mesoporous silica nanoparticles (MSNs-MB),[21] *etc*. The aforementioned composite antioxidants have shown good results in improving the thermal-

* Corresponding authors, E-mail: liufuyong@tyut.edu.cn (F.Y.L.)
E-mail: zhengqiang@zju.edu.cn (Q.Z.)

Received December 4, 2023; Accepted March 11, 2024; Published online April 25, 2024

oxidative aging resistance of SBR. However, due to the limitations of pore volume, the loading efficiency of common carriers for antioxidants is relatively low, with HNTs-RD and MSNs-MB having loading efficiencies of only 2.6 wt% and 3.1 wt%, respectively.[18,21] Fu *et al*.[20]achieved a loading efficiency of 29.7 wt% for antioxidant 4020 by acidifying carbon nanotubes with concentrated sulfuric acid and nitric acid. The thermal-oxidative aging resistance of CNTs-4020/SBR composite were significantly improved, with the fracture elongation retention rate of the material still reaching about 50% after aging for 15 days at 100 °C. However, the addition of CNTs reduced the initial thermal-oxidative aging resistance of SBR, with a decrease of 30% in the fracture elongation retention rate after aging for 1 day at 100 °C. Additionally, CNTs are costly and its pre-loading process is complex and environmentally unfriendly, which limits their large-scale application.

Silica aerogel (SAG), a porous material, boasts a three-dimensional network structure constituted by nano-sized silica particles. The material is renowned for its extraordinary porosity and minimal thermal conductivity.[22,23] Its distinctive nano-framework structure endows SAG with copious pore structures and a remarkably high specific surface area.[24] Since BASF, a German company, pioneered the mass production of SAG,[25] they have been extensively employed for thermal insulation,[26,27] fire resistance and noise reduction,[28] adsorption separation,[29–34] and industrial catalysis,[35,36] among other uses. SAG shares the same chemical composition as fumed silica, and its strong reinforcement capabilities make it a new choice in the field of rubber reinforcement.[37] Lay and his team[38] discovered that integrating SAG into natural rubber (NR) can enhance both the curing characteristics and mechanical properties. Our previous studies[39] indicated that, in comparison to fumed silica, SAG demonstrates a stronger reinforcing effect due to its superior absorption of the bonded rubber. Song *et al*.[40] and Liu *et al*.[41] identified a nano-synergistic effect between silicon-based reinforcing fillers and other reinforcing fillers in rubber. The filler network created by the mixed reinforcing system is more developed, making it more effective at rubber reinforcement.

In this study, *N*-isopropyl-*N*'-phenyl-*p*-phenylenediamine (4010NA), an antioxidant, was dissolved in ethanol and incorporated into the pores of SAG *via* multiple cycles of negative and normal pressure. This resulted in composite particles (A-N) with sustained-release antioxidant and reinforcing capabilities. The effects of these composite particles on the thermal-oxidative aging resistance of SBR vulcanizates were thoroughly examined. This was achieved by comparing the changes in mechanical properties, characteristic functional group content, and crosslinking density of SBR vulcanizates before and after thermal-oxidative aging. The mechanism of thermal-oxidative aging resistance was also analyzed.

EXPERIMENTAL

Materials

The following materials were procured for this study. Styrene-butadiene rubber (SBR1712) from Sinopec Qilu Company, zinc oxide (CR) from Liuzhou Zinc Company, stearic acid from Fengyi Oil and Fat Technology Company, and antioxidant 4010NA (effective component content, 98%) from Shandong Shangshun Chemical Company. Additionally, silica aerogel, with trademark AG-D, was sourced from Huayang New Material Technology Group Co. Ltd., while fumed silica was procured from Cabot (Tianjin). Absolute alcohol (AR) was sourced from Tianjin Tianli Chemical Reagent Co., Ltd.

Preparation of Silica Aerogel-loaded Antioxidant 4010NA Composite Particles

The process for preparing silica aerogel-loaded antioxidant 4010NA composite particles, denoted as "A-N" in this study, is illustrated in Scheme 1. Initially, 4010NA was fully dissolved in anhydrous ethanol. This solution was then thoroughly mixed with silica aerogels. The blend was subjected to a three-cycle process, each cycle comprising a 30-min period under a negative pressure of −0.07 MPa, followed by 15 min at normal pressure. Following these cycles, the sample was purified with ethanol and deionized water to remove any unbound 4010NA. The resulting material was dried in a vacuum oven at a temperature of 60 °C. Upon drying, the product was pulverized into a fine powder to yield the requisite silica aerogel-loaded 4010NA composite particles.

Preparation of Reinforced SBR Composite Materials

According to the formula in Table 1, SBR was subjected to mastication on a two-roll mill (BP-8175-AL, Baopin Precision Instruments, China) through eight passes to ensure uniformity. Subsequently, additives including zinc oxide, stearic acid, reinforcing fillers, DM accelerator, CZ accelerator, and sulfur were added in sequence and mixed thoroughly to achieve a homogeneous blend. This compounded mixture was vulcanized using a flat vulcanizing machine (BP-8170-A, Baopin Precision Instruments, China) at an operating temperature of 160°C and for a duration corresponding to t_{c90}, resulting in sheets with a thickness of 2mm. These sheets were then meticulously cut into dumbbell-shaped specimens in accordance with the ISO 37:2017 standard.

Characterization

Cross-link density measurement

The crosslinking density (V_e) of vulcanizates was tested by

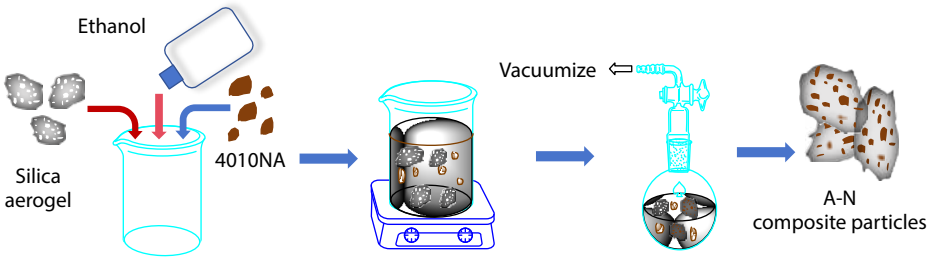

Scheme 1 Schematic illustration of loading antioxidant 4010NA into SAG.

https://doi.org/10.1007/s10118-024-3125-5

Table 1 Formulation of SBR/A-N composites.

Sample	SBR (phr)	A-N (phr)	SAG (phr)	4010NA (phr)	Fumed silica (phr)
S_{45}	100	0	0	0	45
$S_{30}A_{15}$	100	0	15	0	30
$S_{45}N_1$	100	0	0	1	45
$S_{30}A_{15}N_1$	100	0	15	1	30
$S_{30}A_8A\text{-}N_8$	100	8	8	0	30
$S_{30}A_8N_{0.5}A\text{-}N_8$	100	8	8	0.5	30

swelling method.[42] A small piece of vulcanizes was soaked in toluene for 96 h at room temperature. The exact mass of the sample before and after soaking was weighed, and V_e was calculated according to Flory-Rehner equation (Eq. 1).

$$V_e = \left[\ln(1 - V_r) + V_r + XV_r^2\right] / V_0\left(V_r^{1/3} - V_r^{1/2}\right) \quad (1)$$

where V_e is the cross-link density of the rubber (measured in mol/cm³). V_0 is the molar volume of the solvent (expressed in ml/mol). X is the interaction parameter between the rubber and solvent, which is estimated by Eq. (2):

$$X = 0.427 + 0.112V_r^2 \quad (2)$$

where V_r is the volume fraction of rubber in the swollen sample, determined by Eq. (3):

$$V_r = (W_d/\rho) / [W_d/\rho + (W_s - W_d)/\rho_s] \quad (3)$$

The parameters in the formula are defined as follows: ρ_s represents the density of the solvent, denoted in grams per cubic centimeter (g/cm³). W_d refers to the weight of the unaltered rubber specimen, recorded in grams (g). Meanwhile, W_s signifies the weight of the rubber sample post-immersion in the solvent and subsequent drying to eliminate any surface solvent, also quantified in grams (g).

Morphological analysis

The surface morphology of the samples was examined using a scanning electron microscope (GEMINISEM 360, ZEISS, Germany).

Chemical structural analysis

The absorption peaks of the characteristic functional groups of all the samples were characterized by a Fourier-transform infrared spectrometer (INVENIO-S, Bruker Corporation, Germany).

Measurement of loading efficiency of 4010NA on silica aerogel

Thermogravimetric analyzer (TGA2, METTLER TOLEDO, Switzerland) was used to test the thermal weight loss of composite particles in the temperature range of 30–900 °C by a heating rate of 10 °C / min in a nitrogen atmosphere. The loading efficiency (C_a) of 4010NA in SAG was calculated according to Eq. (4),[11]

$$C_a = (1 - w_{A\text{-}N}/w_{SAG}) \times 100\% \quad (4)$$

where $w_{A\text{-}N}$ is weight loss rate (%) of composite particles at 900 °C, w_{SAG} is weight loss rate (%) of raw silica aerogels.

Specific surface area and pore size analysis

The nitrogen adsorption and desorption curves of raw SAG and composite particles were tested at 100 °C by an automatic surface area and porosity analyzer (Quantachrome Autosorb IQ, Quantachrome Instruments U.S, USA). The pore size distribution and specific surface area were analyzed.

Vulcanization characteristics testing of rubber materials

The vulcanization characteristics of rubber compounds were tested by a rotorless vulcanizer (MDR 3000 Basic, MonTech, Germany). The test temperature was 160 °C and the duration time was 60 min.

Mechanical properties testing of rubber vulcanizates before and after aging

Samples after thermal oxidative aging were obtained under the following conditions: In accordance with ISO 188:2011, dumbbell-shaped specimens were placed in a thermal-oxidative aging oven (401B, Yangzhou Tianfa Testing Machinery Co., Ltd., China) at 100 °C within an air atmosphere for various durations.

The tensile properties of the vulcanizate samples before and after aging were tested at room temperature according to ISO 37:2017 using a universal testing machine (UTM4304X, Shenzhen Sansi Zongheng Technology Co. Ltd., China). The tensile speed was set to 500 mm/min.

Glass transition temperature testing of rubber vulcanizates

The glass transition temperature of the rubber vulcanizates, both before and after aging, was characterized using a dynamic thermomechanical analyzer (DMA 242 E Artemis, NETZSCH, Germany).

Surface hydrophobicity testing of rubber materials

The surface hydrophilicity of rubber vulcanizates was characterized using an optical contact angle measuring instrument (DSA100S, KRUSS, Germany).

Other components: Zinc oxide, 5 phr (parts per hundred rubber); Stearic acid, 1 phr; CZ accelerator, 1 phr; DM accelerator, 1 phr; Sulfur, 4 phr.

RESULTS AND DISCUSSION

Loading of 4010NA into Silica Aerogel Pores

Scanning electron microscopy (SEM) was employed to examine the morphology of the SAG and A-N composite particles, as demonstrated in Fig. S1 (in the electronic supplementary information, ESI). It can be observed that the size of the SAG particles used is approximately 3–5 μm. After the loading with 4010NA, the three-dimensional structural morphology of the SAGs remained intact.

To further delve into the possibility of any chemical reactions taking place during the loading of antioxidant 4010NA into the SAG pores, Fourier-transform infrared spectroscopy (FTIR) was performed on both SAG and A-N composite particles. The results of these examinations are exhibited in Fig. S2 (in ESI). As shown in Fig. S2 (in ESI), FTIR curves show the signal of residual small alkanes from the preparation of SAG.[43] The signal of 4010NA[11] indicates that loading remains a physical process, with no chemical interaction transpiring between 4010NA and the hydroxyl groups within SAG.

The antioxidant-silica aerogel (A-N) composite particles utilized in this research were prepared through the process of

https://doi.org/10.1007/s10118-024-3125-5

impregnating SAG with a 4010NA ethanol solution, followed by vacuum treatment. To ascertain the impact of 4010NA concentration within the ethanol solution on the overall loading efficiency, a thermogravimetric analyzer was employed to chart the thermal weight loss curve of the composite particles within a nitrogen environment. The resultant data is illustrated in Fig. 1.

The loading efficiency (C_a) of 4010NA within SAG was determined through the experimental method outlined earlier, as illustrated in Fig. 1(b). An examination of Fig. 1(b) demonstrates that an increase in the concentration of 4010NA in the ethanol solution corresponds to a rise in the C_a of 4010NA in SAG, culminating in a plateau when the concentration surpasses 9%. The maximum C_a of 4010NA in SAG is restricted by the solubility of 4010NA in ethanol and the dispersibility of SAG in the same solution. Within this study, the peak C_a reached was 14.26%, markedly surpassing the antioxidant RD/natural halloysite[18] and antioxidant MB/silica nanotubes[21] systems.

The pore volume and specific surface area of SAG, before and after 4010NA loading, were evaluated using an automated surface area and pore size analyzer. The nitrogen adsorption-desorption isotherms and pore size distribution curves for SAG and A-N composite particles, with varying 4010NA content, are presented in Fig. S3 (in ESI). An analysis of the pore structure data for the different A-N composite particles are shown in Table 2.

Table 2 data suggest a negligible change in the pore volume of SAG post antioxidant adsorption. Nevertheless, there is a consistent reduction in the specific surface area as the micropores begin to be filled, culminating in a plateau when the concentration surpasses 9%. This suggests that the adsorption process is nearing saturation.[44] Subsequent studies will employ a 9% concentration of the antioxidant 4010NA ethanol solution to prepare A-N composite particles with a C_a of 13.4 wt%. These will be utilized to reinforce SBR.

Vulcanization Characteristics of SBR Compounds Filled with A-N Composite Particles

As specified in Table 1, SAG and A-N composite particles were incorporated into SBR as functional fillers to create an SBR compound ($S_{30}A_8A\text{-}N_8$) possessing an anti-emigration effect. All the samples containing A-N mentioned in the article employ the same batch of A-N composite particles with a 4010NA content of 13.4 wt%. When the chosen amount of A-N is 8 phr, the content of 4010NA is approximately 1 phr. Additionally, a small quantity of free 4010NA was introduced to generate an SBR compound ($S_{30}A_8N_{0.5}A\text{-}N_8$), exhibiting both short-term and long-term synergistic anti-thermal oxygen aging effects. Concurrently, four control samples namely S_{45} (containing only fumed silicas), $S_{30}A_{15}$ (containing both fumed silicas and SAG), $S_{45}N_1$ (containing fumed silicas and free 4010NA), and $S_{30}A_{15}N_1$ (containing fumed silicas, SAG, and free 4010NA) were prepared.

The torque curves as a function of time during the vulcanization process for these six compounds were tested at 160 °C, as demonstrated in Fig. 2. The vulcanization characteristic parameters can be derived from the dynamic torque curves, as indicated in Table 3.

Table 3 outlines various key vulcanization parameters for distinct SBR compounds. M_L signifies the torque of the initial rubber compounds, while M_H is generally perceived as the elastic torque upon completion of the rubber compound's thermal vulcanization crosslinking. The discrepancy between M_H and M_L, denoted as ΔM, serves to portray the escalation in the crosslinking degree of the rubber compound. The time at

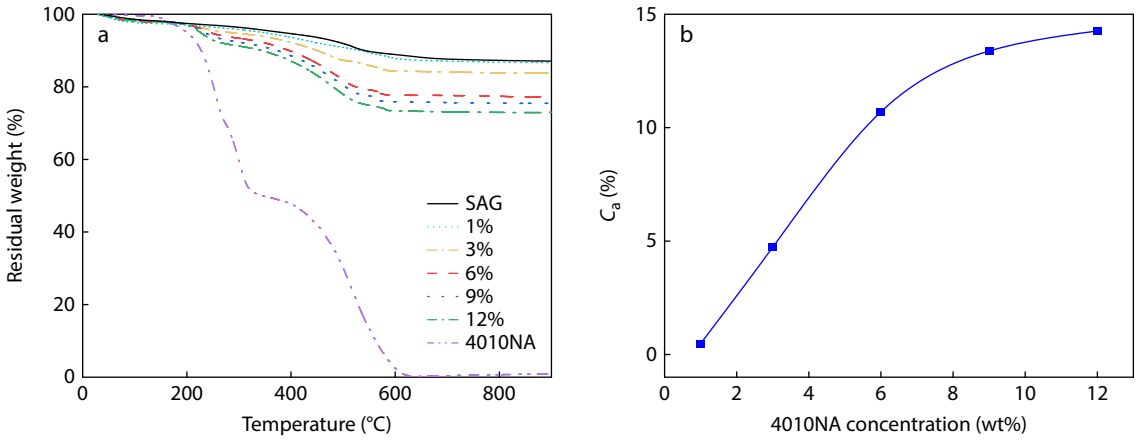

Fig. 1 TGA curves of SAG and A-N composite particles prepared using different concentrations of (a) 4010NA ethanol solution and (b) 4010NA loading efficiency.

Table 2 Characteristic parameters of various A-N composite particles.

Sample	Pore volume ($cm^3 \cdot g^{-1}$)	Specific surface area (cm^2)	Pore diameter (nm)
SAG	0.994	492.73	30.37
3%	1.136	472.94	35.75
6%	1.132	444.70	35.60
9%	1.092	439.89	35.82
12%	1.146	439.62	35.67

https://doi.org/10.1007/s10118-024-3125-5

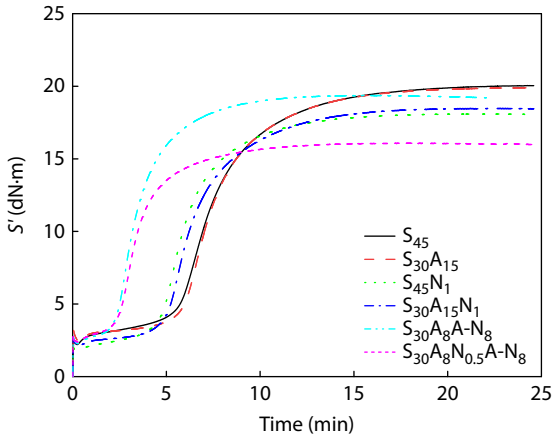

Fig. 2 Time-dependent dynamic torque curves at 160 °C for diverse SBR compounds.

10% vulcanization, referred to as t_{c10} or scorch time, embodies the duration wherein the compound can undergo processing at elevated temperatures. During this stage, the compound's viscosity diminishes without any vulcanization crosslinking, thus facilitating sequential processing operations. Conversely, t_{c90}, or the time at 90% vulcanization, also known as the process vulcanization time, represents the ideal vulcanization duration. A shorter t_{c90} implies heightened rubber vulcanization efficiency, thereby contributing to energy conservation.[45]

Table 3 demonstrates that both t_{c10} and ΔM of S_{45} and $S_{30}A_{15}$, without the inclusion of 4010NA, exceed those of $S_{45}N_1$ and $S_{30}A_{15}N_1$, which incorporate free 4010NA. This suggests that the integration of free 4010NA curtails the operating time of the rubber compound and lessens the extent of crosslinking enhancement. During the vulcanization process of the rubber compound, a vulcanization system comprising sulfur and accelerator generates polysulfide active free radicals due to heat. These radicals instigate the reaction of rubber molecules, leading to the formation of macromolecules with polysulfide accelerator side groups. Subsequently, crosslinked bonds are formed between the active side groups and the rubber molecules.[46] Furthermore, 4010NA, as an amine antioxidant, acts as an external ligand during the rubber vulcanization process. It occupies the vacant zinc orbitals, diminishing the strength of the Zn-S bonds.[47] This increases the nucleophilicity of the thiol sulfur atoms and facilitates the production of active vulcanizing agents, which consequently reduces the scorch time of rubber compound. During the latter stages of vulcanization, 4010NA exhibits a superior capture efficiency for free radicals, reacting with sulfur-active radicals generated by the vulcanization system. This decreases the likelihood of cross-link bonds forming between sulfur-active radicals and rubber molecules, thereby reducing ΔM.

The incorporation of A-N composite particles notably decreases t_{c10} without a significant reduction in ΔM. The subsequent introduction of free 4010NA to $S_{30}A_8A\text{-}N_8$ results in a further diminution of both t_{c10} and ΔM. This is attributed to the fact that when antioxidant 4010NA is integrated into the pores of SAG, it is predominantly bound by SAG, resulting in a

Table 3 Vulcanization characteristic parameters of different SBR compounds.

Sample	M_H (dN·m)	M_L (dN·m)	t_{c10} (min)	t_{c90} (min)	ΔM (dN·m)
S_{45}	20.10	2.21	4.84	12.26	17.89
$S_{30}A_{15}$	19.92	2.45	5.49	11.99	17.47
$S_{45}N_1$	18.09	1.79	4.24	9.75	16.30
$S_{30}A_{15}N_1$	18.47	2.12	4.71	10.87	16.35
$S_{30}A_8A\text{-}N_8$	19.37	2.28	2.27	6.59	17.09
$S_{30}A_8N_{0.5}A\text{-}N_8$	16.07	2.40	2.25	6.62	13.67

Note: M_H, maximum torque; M_L, minimum torque; t_{c10}, time at 10% vulcanization; t_{c90}, time at 90% vulcanization; $\Delta M = M_H - M_L$.

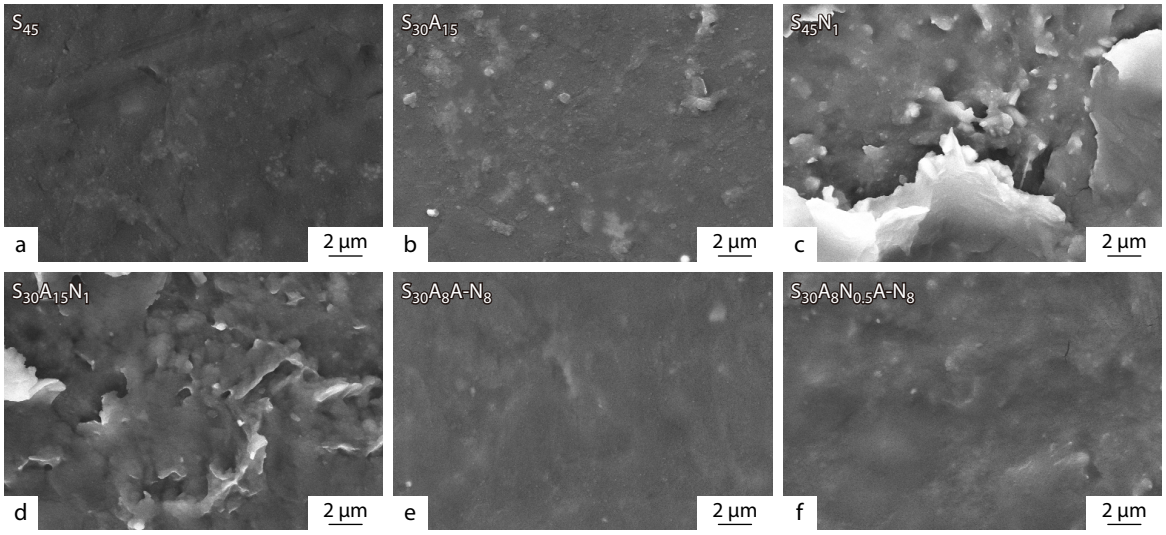

Fig. 3 SEM micrographs detailing the surface morphology of SBR/A-N vulcanizates placed for 60 days at ambient temperature.

https://doi.org/10.1007/s10118-024-3125-5

more evenly distributed dispersion within the system and consequently leading to a further decrease in t_{c10}. The confinement of 4010NA within the pores substantially minimizes its decomposition during processing, consequently mitigating its detrimental effects on cross-linking. Further addition of free 4010NA to $S_{30}A_8A\text{-}N_8$ can reduce its t_{c10} and ΔM even more.

Anti-Frosting Performance of A-N Reinforced SBR Vulcanizates

The extensive incorporation of antioxidants in conventional rubber formulations leads their migration to the surface of vulcanizates, resulting in the phenomenon of frosting that markedly impairs the mechanical properties. These antioxidants are typically low-molecular-weight, hydrophobic compounds whose accumulation at the vulcanized rubber's surface augments its hydrophobicity—a factor that inversely correlates with anti-frosting efficacy.[48] To evaluate this aspect, the water contact angle on the surface of six sets of SBR vulcanizates, placed for 60 days, was measured. The results are depicted in Fig. S4 (in ESI). Concurrently, the surface morphology of these vulcanizates was examined using SEM, with the micrographs presented in Fig. 3.

The SEM images demonstrate that the surfaces of S_{45} and $S_{30}A_{15}$, devoid of unbound 4010NA, are notably smooth, suggesting an absence of antioxidant migration. In contrast, the surfaces of $S_{45}N_1$ and $S_{30}A_{15}N_1$ exhibit layered aggregates, indicative of migrated antioxidants. However, $S_{30}A_8A\text{-}N_8$ and $S_{30}A_8N_{0.5}A\text{-}N_8$ retain their smoothness, implying negligible antioxidant migration.

The hierarchy of water contact angles among the six groups of samples, in descending order, is $S_{45}N_1$, $S_{30}A_{15}N_1$, $S_{30}A_8N_{0.5}A\text{-}N_8$, $S_{30}A_{15}$, $S_{30}A_8A\text{-}N_8$, and S_{45}. The SAG employed in these formulations contains residual organic constituents, contributing to a degree of hydrophobicity that results in a greater water contact angle for $S_{30}A_{15}$ compared to S_{45}. The hydrophobic organic compound 4010NA, when migrated to the vulcanizate's surface, further enhances hydrophobicity, as evidenced by the highest contact angle observed in $S_{45}N_1$. The marginally lower angle in $S_{30}A_{15}N_1$ is attributed to partial adsorption of free 4010NA by the SAG. The surface of $S_{30}A_8A\text{-}N_8$ is largely free of migrated antioxidants owing to the robust binding affinity of SAG, which is reflected in a water contact angle only slightly elevated compared to the antioxidant-free S_{45}. For $S_{30}A_8N_{0.5}A\text{-}N_8$, the presence of additional unbound antioxidant increases the contact angle beyond that of $S_{30}A_8A\text{-}N_8$, as the saturated A-N composite particles are incapable of adsorbing the excess antioxidants.

Thermal-oxidative Aging Resistance of A-N Reinforced SBR Vulcanizates

The six SBR compounds previously described were subjected to thermal vulcanization at 160 °C, utilizing a t_{c90}+5 min protocol, to yield a series of vulcanized SBR materials. These vulcanizates

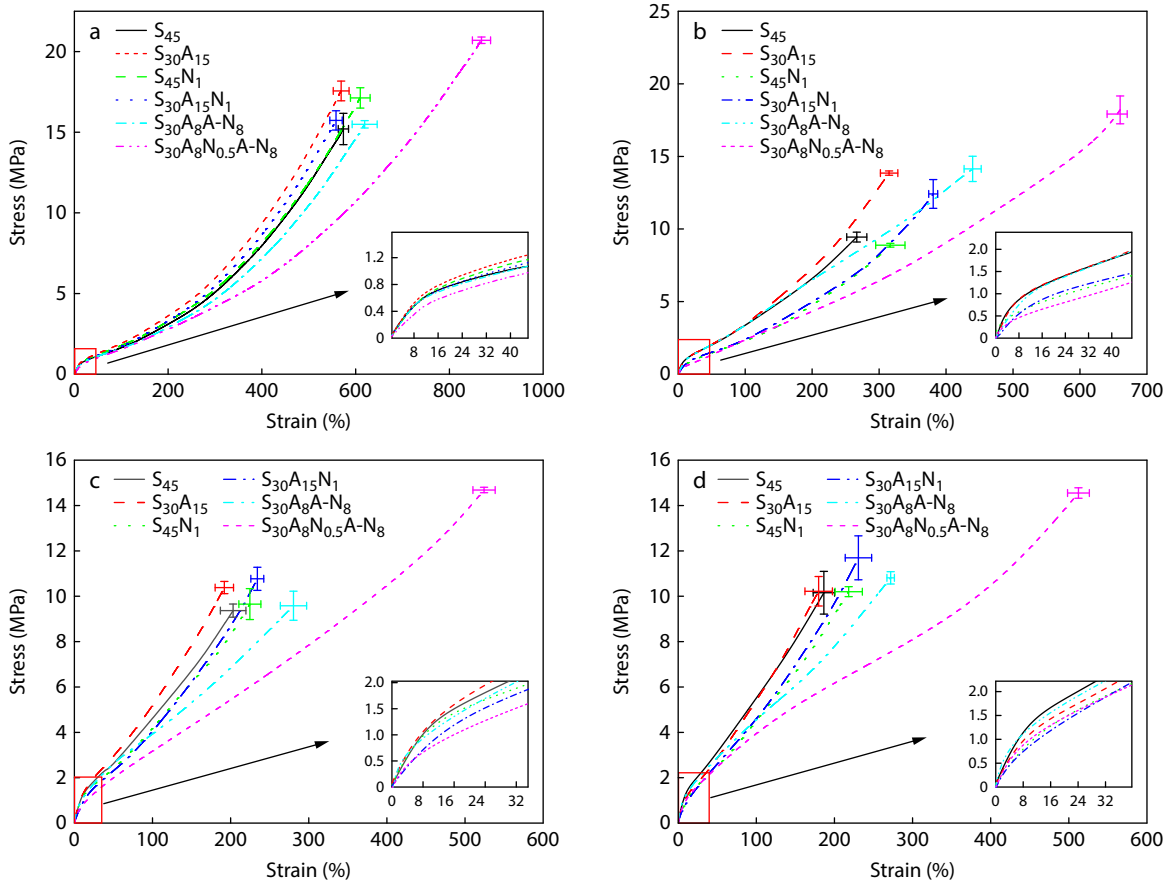

Fig. 4 The original stress-strain curves of SBR/A-N vulcanizates before and after thermal-oxidative aging at 100 °C for various period (a: 0 h; b: 24 h; c: 72 h; d: 96 h).

https://doi.org/10.1007/s10118-024-3125-5

were fashioned into dumbbell-shaped specimens and subjected to thermal-oxidative aging at 100 °C for varying durations (24 h, 72 h, 96 h) within a controlled aging chamber.

The original stress-strain curves for six sets of samples before and after aging for various durations are shown in Fig. 4. The tensile modulus calculated from the initial linear region of the stress-strain curves (embedded in Fig. 4), including the stress at 100%, is presented in Fig. 5. The variations in tensile strength, elongation at break, and their retention rates with thermal-oxidative aging time are illustrated in Fig. 6. Fig. 6 also depicts the Shore A hardness (Fig. 6c) and its retention rate (Fig. 6f).

From Figs. 4–6, it can be observed that, under low strain conditions (<100%), the stress-strain curves of different samples before aging are essentially the same. With increasing strain, different filler systems exhibit varying strain-hardening effects. The $S_{30}A_{15}$ sample, without any antioxidants, shows the highest stress increase among all samples, indicating the excellent reinforcing effect of SAG.[49,50] The sample incorporating both A-N and free antioxidants ($S_{30}A_8N_{0.5}A\text{-}N_8$) exhibits the smallest stress increase during strain growth, ultimately achieving the maximum elongation at break and the highest tensile strength. The elongation at break is significantly superior to those of SBR vulcanizates filled with HNTs (450.39%)[18] and carbon black/MSN-SH (480.35%).[11,19] This is attributed to the synergistic effect of amine antioxidants inhibiting SBR cross-linking[51,52] and the high reinforcing effect of SAG.

After undergoing aging at 100 °C for 24 h, the sample

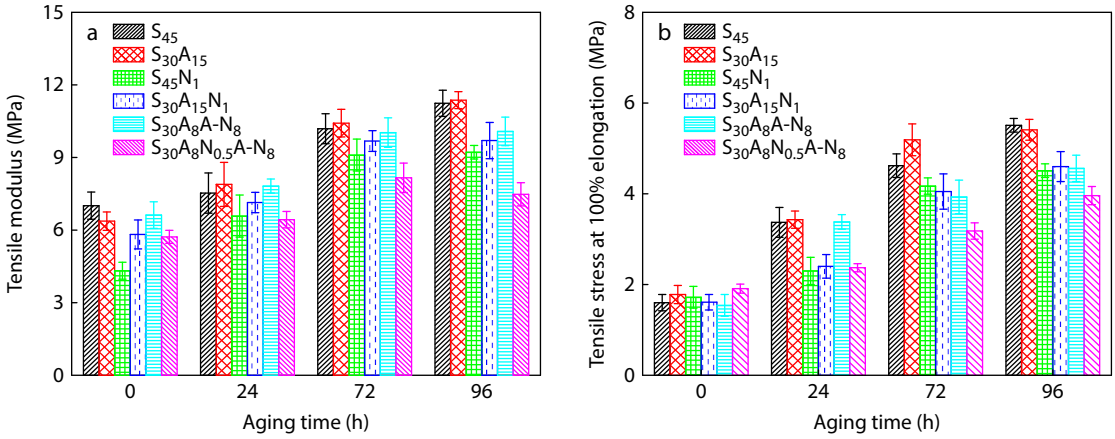

Fig. 5 The tensile modulus (a) and stress at 100% (b) of SBR/A-N vulcanizates before and after thermal-oxidative aging at 100 °C for various timeframes.

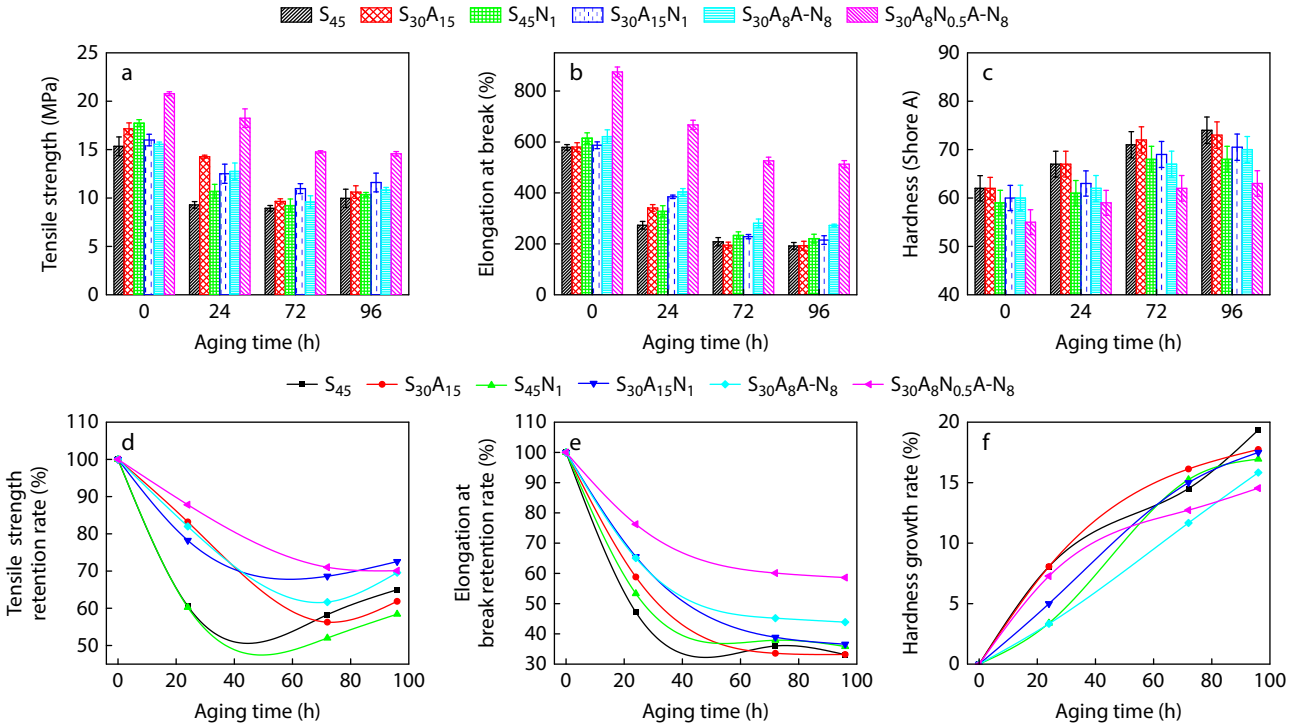

Fig. 6 (a–c) Mechanical properties, (d, e) retention rates, and (f) the rate of increase in hardness of SBR/A-N vulcanizates before and after thermal-oxidative aging at 100 °C for various timeframes.

https://doi.org/10.1007/s10118-024-3125-5

$S_{30}A_{15}$ demonstrates a more significant enhancement in tensile modulus relative to sample S_{45}. Conversely, the rise in tensile stress at 100% elongation for $S_{30}A_{15}$ is less marked. Consequently, $S_{30}A_{15}$ surpasses S_{45} in maintaining tensile strength and elongation at break by margins of 22.65% and 11.64%, respectively. This is attributed to the high structural integrity of SAG, making the interaction between SAG and SBR more robust and less prone to disruption. The addition of SAG enhances the early-stage thermal-oxidative aging resistance of SBR, which is not observed in carbon nanotube (CNT)-reinforced SBR.[20] The strong adsorption of antioxidants by CNTs prevents effective release in the early stages of aging, causing a rapid decline in performance during the initial aging period.[20] Except for the $S_{30}A_8N_{0.5}A\text{-}N_8$ sample, the tensile strength of other samples initially decreases and then rises with prolongation of aging time, which is a characteristic aging behavior of SBR.[53] During the aging process of SBR, degradation and cross-linking occur simultaneously. Initially, the rubber molecular chains undergo only mild thermal degradation without significant cross-linking. As aging progresses, the cross-linking density between rubber molecular chain segments increases, leading to a notable rise in the rubber's tensile modulus and, consequently, a significant increase in the elastic modulus. This results in enhanced tensile strength and hardness of the rubber, but a precipitous decline in the elongation at break. Therefore, with the extension of aging time, the S_{45} and $S_{30}A_{15}$ samples, which did not include any anti-aging agents, exhibited a more rapid increase in tensile stress at 100% elongation and tensile modulus (Fig. 5) as well as in Shore A hardness (Fig. 6c), along with a sharp decrease in elongation at break (Fig. 6b), compared to the other samples.

After aging at 100 °C for 96 h, the $S_{30}A_8A\text{-}N_8$ sample containing A-N retained 43.88% of its initial elongation at break, which is higher than the 33% for the control group S_{45} and $S_{30}A_{15}$, and 36% for $S_{45}N_1$ and $S_{30}A_{15}N_1$. This is attributed to the continuous and sustained release of antioxidants from the mesopores of SAG as aging time increases. In the case of the sample $S_{30}A_8N_{0.5}A\text{-}N_8$, which contains both free antioxidants and A-N, free antioxidants are consumed in the early stages of aging. In the subsequent aging process, encapsulated 4010NA within the A-N composite continues to be released, mitigating further cross-linking of the rubber molecular chains and efficiently maintaining the elongation at break of the sample (elongation at break retention of 58.61% after 96 h of aging), reducing the increase in hardness. Consequently, this minimizes the decrease in tensile strength to the maximum extent.

Thermal-oxidative Aging Mechanism of A-N Reinforced SBR Vulcanizates

The thermal-oxidative degradation of rubber typically proceeds as follows (refer to Scheme 2, upper portion), when exposed to high heat and oxygen-rich environments. Rubber molecules contain oxidizable groups such as carbon-carbon double bonds and methyl or methylene groups, which are prone to oxygen attack under thermal effect. This leads to fragmentation of molecular chain and the formation of carbon radicals. These radicals are further oxidized, abstracting hydrogen from carbon-hydrogen bonds to yield hydroperoxides, which subsequently decompose to generate oxygen-containing functionalities, including carboxyl and alkoxy groups.[2,54,55] Notably, at elevated temperatures, alkoxy groups can cleave to form carbonyl groups with carbon-oxygen double bonds.[56]

To investigate the thermal-oxidative aging resistance of SBR/A-N vulcanizates, we performed infrared spectroscopy testing on six sets of samples subjected to aging over varied durations. The infrared spectra of these sample at different aging intervals are presented in Fig. S5 (in ESI). For a clearer representation of the thermal-oxidative aging resistance, we computed the carbonyl index (CI) as shown in Figs. 7(a) and 7(b), using Eq. (5),[57] and the methylene retention rate as displayed in Fig. 7(c).

$$CI = A_{1709cm^{-1}}/A_{1447cm^{-1}} \times 100\% \quad (5)$$

Fig. 7(a) illustrates that the CI values for samples aged at 100 °C for seven days remained relatively unchanged. This is because 100 °C is not high enough to expediting oxidative reactions in the SBR matrix.[58,59] According to the principles outlined by the Arrhenius equation,[60] an increase in temperature can expedite the oxidative reactions of materials and enhance the detection of characteristic functional groups. As

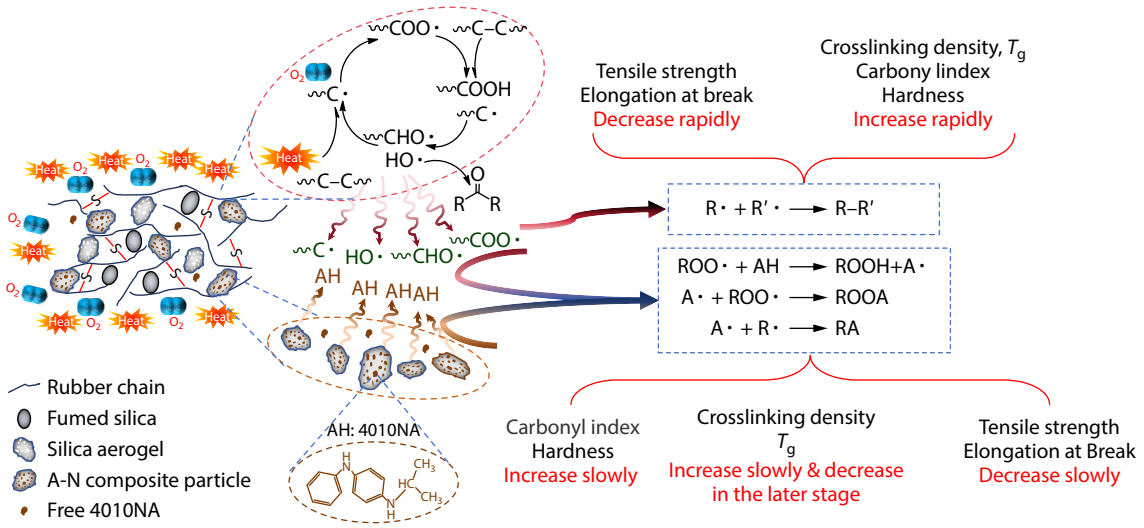

Scheme 2 The mechanism of A-N releasing antioxidant and improving the thermal oxidative aging resistance of SBR vulcanizate.

https://doi.org/10.1007/s10118-024-3125-5

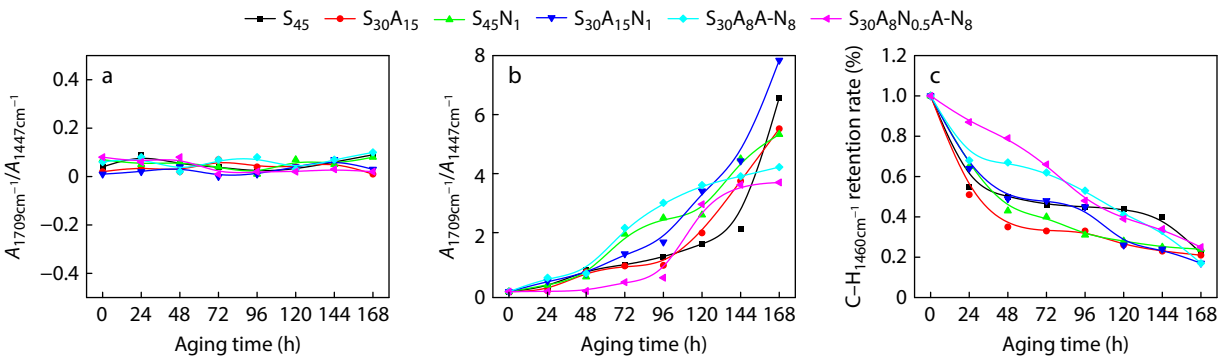

Fig. 7 Changes in characteristic functional group parameters of SBR/A-N vulcanizates with aging time. (a) Variation of CI values with aging time at 100 °C; (b) Variation of CI values with aging time at 150 °C; (c) Variation of methylene retention rate at 1447 cm^{-1} with aging time at 150 °C.

illustrated in Fig. 7(b), the CI for all six groups of samples exhibit a pattern of initial increase to a plateau phase, followed by a continual rise. However, the duration required to reach this plateau varies among the samples. Specifically, the CI for S_{45} and $S_{30}A_{15}$ stabilized at the plateau after 24 h of aging, $S_{45}N_1$ and $S_{30}A_{15}N_1$ after 72 h, and $S_{30}A_8N_{0.5}A\text{-}N_8$ after 120 h. Throughout the 168-hour testing period, the CI of the samples containing A-N, namely $S_{30}A_8A\text{-}N_8$ and $S_{30}A_8N_{0.5}A\text{-}N_8$, did not display any further increase after reaching the initial plateau.

The trend of methylene retention rates during aging at 150 °C, depicted in Fig. 7(c), reveals that the oxidation of methylene groups in samples S_{45}, $S_{30}A_{15}$, $S_{45}N_1$, and $S_{30}A_{15}N_1$ can be categorized into three phases: an initial marked decrease, a stable intermediate stage, and a subsequent pronounced decline. By contrast, $S_{30}A_8A\text{-}N_8$ and $S_{30}A_8N_{0.5}A\text{-}N_8$ show a more gradual and consistent reduction in methylene retention rates, without clear demarcation into distinct phases of oxidation. Furthermore, the retention rates of elongation at break indicates that $S_{30}A_8A\text{-}N_8$ and $S_{30}A_8N_{0.5}A\text{-}N_8$ undergo a more uniform decline compared to their counterparts. This triphasic reduction in methylene content during the thermal-oxidative aging of SBR correlates with the thermal oxidation susceptibility of the butadiene units, which follows the reactivity sequence: vinyl > *trans*-1,4-polybutadiene > *cis*-1,4-polybutadiene. Thermal-oxidative degradation typically progresses by sequentially consuming the most susceptible groups.[56]

During thermal-oxidative aging, the extensive generation of free radicals from molecular chain scission prompts increased cross-linking. This augmentation of cross-link density curtails the mobility of polymer chain segments, diminishing their flexibility, which can be evidenced by an elevation in the glass transition temperature (T_g).[61] Investigating changes in T_g, which reflect the crosslinking density in vulcanizates at varying stages of aging, can elucidate the mechanisms by which A-N composite particles enhance the thermal-oxidative resistance of SBR. Dynamic mechanical analysis (DMA) was performed on six sample sets. The dependence of the loss factor tangent (tanδ) on temperature for the unaged samples is depicted in Fig. 8(a), where the T_g corresponds to the peak of the curve.[62] The tanδ variation with temperature of the samples aged at 100 °C for varying durations is illustrated in Fig. S6 (in ESI), alongside the T_g progression with aging time in Fig. 8(b).

As indicated in Fig. 8(a), the samples with 4010NA antioxidant ($S_{45}N_1$ and $S_{30}A_{15}N_1$) exhibit a marginal increase in T_g in comparison to S_{45} and $S_{30}A_{15}$. This rise may be attributable to the intramolecular cross-linking induced by amine-type antioxidants during rubber vulcanization, which constrains flexibility.[63] The incorporation of A-N composite particles in $S_{30}A_8A\text{-}N_8$ further amplifies the T_g, likely due to the physically induced cross-linking by the well-dispersed A-N particles. Conversely, $S_{30}A_8N_{0.5}A\text{-}N_8$ with free antioxidants demonstrates a slight T_g decrement yet remains substantially higher

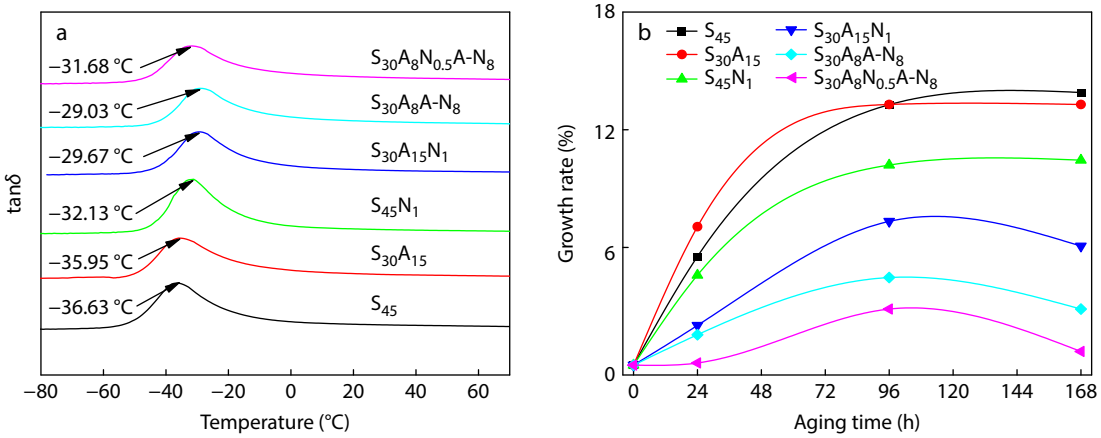

Fig. 8 (a) tanδ-temperature curves for the unaged samples and (b) the T_g evolution rate with aging time for the six sets of samples.

https://doi.org/10.1007/s10118-024-3125-5

than $S_{30}A_{15}$.

Moreover, the impact of thermal-oxidative aging on the T_g of different samples was assessed. The tanδ transitions with temperature for the six aged samples are presented in Fig. S6 (in ESI), and the corresponding T_g growth rates with aging time are depicted in Fig. 8(b). Initial aging stages show a general T_g increase across all samples, as seen in Fig. 8(b). After 96 h of aging, the T_g for S_{45} and $S_{30}A_{15}$ samples devoid of antioxidants increased to the plateau period, showing no further change with increased aging time. The T_g trajectory of $S_{45}N_1$ parallels this trend, albeit with a smaller increment. After 168 h of aging, the T_g for $S_{30}A_{15}N_1$ and samples containing A-N composite particles exhibits a decline.

During the thermal-oxidative aging of SBR, concurrent chain scission and cross-linking significantly modify the polymer's molecular structure. It has been observed that re-crosslinking during aging primarily contributes to the rise in the T_g and the associated changes in mechanical properties.[64,65] The T_g growth rate for $S_{45}N_1$ and $S_{30}A_{15}N_1$ samples is lower than that for S_{45} and $S_{30}A_{15}$, suggesting that the incorporation of free 4010NA antioxidant can somewhat inhibit SBR molecular re-crosslinking during aging, thereby decelerating the rubber's hardening process. The inclusion of A-N composite particles further reduces the T_g growth rate and substantially lowers T_g after 168 h of aging, indicating that A-N composites can more effectively retard the aging-related cross-linking of SBR molecules than free antioxidants alone. Furthermore, A-N composites provide a more sustained aging protection, evidenced by a decrease in T_g during the later stages of aging.

To intuitively assess changes in the crosslinking density (V_e) of samples before and after thermal-oxidative aging, V_e was tested through equilibrium swelling methods and the results were normalized and presented in Fig. 9.

In the initial stage of aging, all six sets of samples exhibited a rapid increase in V_e corresponding with the duration of aging. Nonetheless, the V_e increase for $S_{45}N_1$ and $S_{30}A_{15}N_1$ was less pronounced than that for S_{45} and $S_{30}A_{15}$ throughout the aging process. In contrast, samples containing A-N composites ($S_{30}A_8A\text{-}N_8$) and those with both free antioxidants and A-N composites ($S_{30}A_8N_{0.5}A\text{-}N_8$) showed a reduction in V_e after aging 100 h. This trend is in line with the aforementioned T_g observations, reinforcing the premise that crosslinking predominates as the key reaction mechanism for SBR molecular chains during the later stages of thermal-oxidative aging.

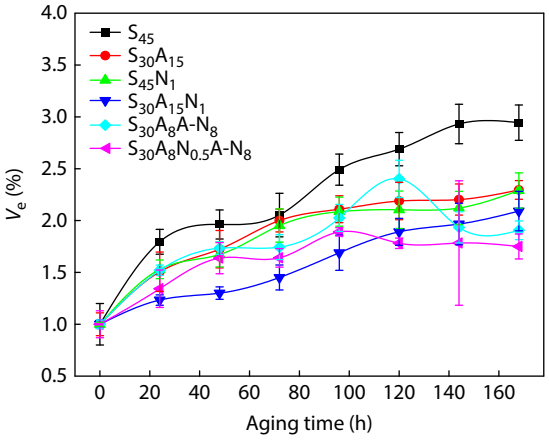

Fig. 9 Variation of crosslink density (V_e) with aging time for six groups of samples.

During the aging process of rubber, antioxidants play a crucial role in mitigating the increase of V_e by scavenging free radicals. As a result, samples S_{45} and $S_{30}A_{15}$, which lack antioxidants, exhibit a rise in Ve that correlates with the duration of aging. Conversely, samples $S_{45}N_1$ and $S_{30}A_{15}N_1$, containing free antioxidants, show a reduced rate of V_e increase, attributable to the antioxidants' radical-capturing activity. The samples $S_{30}A_8A\text{-}N_8$ and $S_{30}A_8N_{0.5}A\text{-}N_8$, with a lower content of free antioxidants compared to $S_{30}A_{15}N_1$, exhibit a less pronounced inhibition of the cross-linking reaction in the initial stages of aging. Consequently, the early aging stage sees a more significant increase in V_e for these samples than for $S_{30}A_{15}N_1$. However, as the aging progresses, the sustained release of antioxidants from the A-N composites maintains the inhibition of cross-linking. In the latter stages, the degradation of macromolecules becomes more pronounced, leading to a progressive reduction in the V_e of $S_{30}A_8A\text{-}N_8$ and $S_{30}A_8N_{0.5}A\text{-}N_8$.

In summary, the thermal-oxidative aging resistance mechanism of SBR reinforced by A-N composite particle can be illustrated as in Scheme 2. The presence of A-N composite particles, in tandem with a smaller quantity of free antioxidants, markedly prevented the oxidation of methylene groups and the rupture of carbon-carbon bonds within the SBR molecular chains during the initial stage of thermal-oxidative aging. In the subsequent stage, the gradual release of the encapsulated antioxidants captured and neutralized a large proportion of radicals generated during aging, thereby significantly inhibiting further cross-linking and delaying the onset of hardening and embrittlement in the vulcanizates.

CONCLUSIONS

In this study, silica aerogels (SAG) were utilized as carriers to develop composite particles that serve dual functions: sustained release of antioxidants and reinforcement of the polymer matrix. Incorporating these composite particles into the styrene-butadiene rubber (SBR) matrix enhanced the antioxidant concentration by 150% without any observable migration. This augmentation resulted in significant enhancements in the mechanical properties of the SBR vulcanizates evidenced by the fact that, the tensile strength and elongation at break of vulcanizates containing A-N composite particles ($S_{30}A_8N_{0.5}A\text{-}N_8$) were increased by 17.5% and 41.9%, respectively, in contrast to those with fumed silica and unencapsulated antioxidants ($S_{45}N_1$).

Most notably, the addition of 4010NA-loaded SAG markedly improved the thermal-oxidative aging resistance of the SBR vulcanizates. After 96 hours of aging, the tensile strength and elongation at break of $S_{30}A_8N_{0.5}A\text{-}N_8$ samples retained 70.09% and 58.61% of their original values, respectively. Compared to the $S_{45}N_1$ samples, the retention rate of elongation at break was 62.8% higher, signifying that the A-N composite particles effectively curtailed the intermolecular cross-linking reactions that typically occur in the later stages of thermal-oxidative aging.

https://doi.org/10.1007/s10118-024-3125-5

Conflict of Interests

The authors declare no interest conflict.

Electronic Supplementary Information

Electronic supplementary information (ESI) is available free of charge in the online version of this article at http://doi.org/10.1007/s10118-024-3125-5.

Data Availability Statement

The data that support the findings of this work are available from the corresponding author on reasonable request. The authors' contact information: liufuyong@tyut.edu.cn (F.Y.L.), zhengqiang@zju.edu.cn (Q.Z.).

ACKNOWLEDGMENTS

This work was financially supported by Natural Science Foundation of Shanxi Province (No. 202303021211075), Shanxi Province Science and Technology Key Research and Development Project (No. 201903D321065) and Shanxi-Zheda Institute of Advanced Materials and Chemical Engineering (No. 2021SX-TD011).

REFERENCES

1 Aprem, A. S.; Joseph, K.; Thomas, S. Recent developments in crosslinking of elastomers. *Rubber Chem. Technol.* **2005**, *78*, 458–488.
2 Li, G.-Y.; Koenig, J. L. A review of rubber oxidation. *Rubber Chem. Technol.* **2005**, *78*, 355–390.
3 Zhao, W.; He, J.; Yu, P.; Jiang, X.; Zhang, L. Recent progress in the rubber antioxidants: a review. *Polym. Degrad. Stabil.* **2023**, *207*, 110223.
4 Ji, Y.; Han, S. D.; Wu, H.; Guo, S. Y.; Zhang, F. S.; Qiu, J. H. Understanding the thermal impedance of silicone rubber/hexagonal boron nitride composites as thermal interface materials. *Chinese J. Polym. Sci.* **2024**, *42*, 352–363.
5 Tayefi, M.; Eesaee, M.; Hassanipour, M.; Elkoun, S.; David, E.; Nguyen-Tri, P. Recent progress in the accelerated aging and lifetime prediction of elastomers : a review. *Polym. Degrad. Stabil.* **2023**, *214*, 110379–21.
6 Liu, Q.; Wei, P.; Cong, C.; Meng, X.; Zhou, Q. Synthesis and antioxidation behavior in EPDM of novel macromolecular antioxidants with crosslinking and antioxidation effects. *Polym. Degrad. Stabil.* **2022**, *205*, 110155.
7 Choi, S. S.; Im, S. H.; Park, J. H.; Kim, J. S. Analysis of wax solubility of rubber vulcanizates using wax solution in toluene and molten wax. *Polym. Test.* **2009**, *28*, 696–701.
8 Bom, N. M.; Usuda, E. O.; da Silva Gigliotti, M.; de Aguiar, D. J. M.; Imamura, W.; Paixao, L. S.; Carvalho, A. M. G. Waste tire rubber-based refrigerants for solid-state cooling devices. *Chinese J. Polym. Sci.* **2020**, *38*, 769–775.
9 Choi, S. S.; Chung, H. S.; Joo, Y. T.; Min, B. K.; Lee, S. H. Analysis of the whitening phenomenon of a thermoplastic elastomer article by UV weathering. *Polym. Test.* **2011**, *30*, 415–419.
10 Choi, S. S.; Chung, H. S.; Joo, Y. T.; Yang, K. M.; Lee, S. H. Analysis of whitening phenomenon of EPDM article by humid aging. *J. Appl. Polym. Sci.* **2012**, *123*, 2451–2457.
11 Fu, Y.; Zhao, D.; Yao, P.; Wang, W.; Zhang, L.; Lvov, Y. Highly aging-resistant elastomers doped with antioxidant-loaded clay nanotubes. *ACS Appl. Mater. Interfaces* **2015**, *7*, 8156–8165.
12 Dileep, P.; Narayanankutty, S. K. Styrenated phenol modified nanosilica for improved thermo-oxidative and mechanical properties of natural rubber. *Polym. Test.* **2020**, *82*, 106302.
13 Zhong, B.; Dong, H.; Luo, Y. Antioxidant modified graphene oxide for robust and highly aging resistant rubber composites. *Compos. Commun.* **2023**, *37*, 101443–101446.
14 Zhang, L.; Li, H.; Lai, X.; Liao, X.; Wang, J.; Su, X.; Liu, H.; Wu, W.; Zeng, X. Functionalized graphene as an effective antioxidant in natural rubber. *Compos. Part A-Appl. S* **2018**, *107*, 47–54.
15 Lu, Y.; Yang, J.; Yin, D.; Tan, M.; Wang, J. Synthesis and aging properties of reactive antioxidant NAPM in natural rubber vulcanizates. *J. Appl. Polym. Sci.* **2008**, *108*, 576–582.
16 Wu, W.; Zeng, X.; Li, H.; Lai, X.; Xie, H. Synthesis and antioxidative properties in natural rubber of novel macromolecular hindered phenol antioxidants containing thioether and urethane groups. *Polym. Degrad. Stabil.* **2015**, *111*, 232–238.
17 Xie, H.; Li, H.; Lai, X.; Wu, W.; Zeng, X. Synthesis and antioxidative properties of a star-shaped macromolecular antioxidant based on β-cyclodextrin. *Mater. Lett.* **2015**, *151*, 72–74.
18 Zhong, B.; Lin, J.; Liu, M.; Jia, Z.; Luo, Y.; Jia, D.; Liu, F. Preparation of halloysite nanotubes loaded antioxidant and its antioxidative behaviour in natural rubber. *Polym. Degrad. Stabil.* **2017**, *141*, 19–25.
19 Luo, Y.; Wang, J.-P.; Cui, X.; Fu, Y.; Li, G. L.; Wang, W. Surface-modified mesoporous silica nanorods for the highly aging resistance rubber through controlled release of antioxidant. *Polym. Adv. Technol.* **2021**, *32*, 3384–3391.
20 Fu, Y.; Yang, C.; Lvov, Y. M.; Zhang, L.; Wang, W. Antioxidant sustained release from carbon nanotubes for preparation of highly aging resistant rubber. *Chem. Eng. J.* **2017**, *328*, 536–545.
21 Hu, D.; Luo, Y.; Chen, Y.; Lin, J.; Jia, D. Mesoporous silica as nanocarrier of antioxidant for highly anti-aging elastomer composites. *Polym. Degrad. Stabil.* **2019**, *169*, 108987–108995.
22 Zhao, S.; Siqueira, G.; Drdova, S.; Norris, D.; Ubert, C.; Bonnin, A.; Galmarini, S.; Ganobjak, M.; Pan, Z.; Brunner, S.; Nyström, G.; Wang, J.; Koebel, M. M.; Malfait, W. J. Additive manufacturing of silica aerogels. *Nature* **2020**, *584*, 387–392.
23 Linhares, T.; Pessoa de Amorim, M. T.; Durães, L. Silica aerogel composites with embedded fibres: a review on their preparation, properties and applications. *J. Mater. Chem. A* **2019**, *7*, 22768–22802.
24 Kistler, S. S. Coherent expanded-aerogels. *J. Phys. Chem.* **2002**, *36*, 52–64.
25 Bheekhun, N.; Abu Talib, A. R.; Hassan, M. R. Aerogels in aerospace: an overview. *Adv. Mater. Sci. Eng.* **2013**, *2013*, 1–18.
26 Eskandari, N.; Motahari, S.; Atoufi, Z.; Hashemi Motlagh, G.; Najafi, M. Thermal, mechanical, and acoustic properties of silica-aerogel/UPVC composites. *J. Appl. Polym. Sci.* **2017**, *134*, 44685.
27 Sun, G.; Duan, T.; Liu, C.; Zhang, L.; Chen, R.; Wang, J.; Han, S. Fabrication of flame-retardant and smoke-suppressant isocyanate-based polyimide foam modified by silica aerogel thermal insulation and flame protection layers. *Polym. Test.* **2020**, *91*, 106738.
28 Fricke, J.; Tillotson, T. Aerogels: production, characterization, and applications. *Thin Solid Films* **1997**, *297*, 212–223.
29 Zhou, S.; You, T.; Zhang, X.; Xu, F. Superhydrophobic cellulose nanofiber-assembled aerogels for highly efficient water-in-oil emulsions separation. *ACS Appl. Nano Mater.* **2018**, *1*, 2095–2103.
30 Zheng, X.; Liu, X.; Zha, L. Under-oil superhydrophilic poly(vinyl alcohol)/silica hybrid nanofibrous aerogel for gravity-driven separation of surfactant-stabilized water-in-oil emulsions. *Macromol. Mater. Eng.* **2019**, *304*, 1900125–1900129.

31 Mazrouei-Sebdani, Z.; Salimian, S.; Khoddami, A.; Shams-Ghahfarokhi, F. Sodium silicate based aerogel for absorbing oil from water: the impact of surface energy on the oil/water separation. *Mater. Res. Express* **2019**, *6*, 085059.

32 Wang, Q.; Asoh, T. A.; Uyama, H. Facile fabrication of flexible bacterial cellulose/silica composite aerogel for oil/water separation. *Bull. Chem. Soc. Jpn.* **2018**, *91*, 1138–1140.

33 Zhang, Y.; Shen, Q.; Li, X.; Xie, H.; Nie, C. Facile synthesis of ternary flexible silica aerogels with coarsened skeleton for oil-water separation. *RSC Adv.* **2020**, *10*, 42297–42304.

34 Liu, H.; Sha, W.; Cooper, A. T.; Fan, M. Preparation and characterization of a novel silica aerogel as adsorbent for toxic organic compounds. *Colloids Surf. Physicochem. Eng. Aspects* **2009**, *347*, 38–44.

35 Ganonyan, N.; Bar, G.; Gvishi, R.; Avnir, D. Gradual hydrophobization of silica aerogel for controlled drug release. *RSC Adv.* **2021**, *11*, 7824–7838.

36 Giray, S.; Bal, T.; Kartal, A. M.; Kızılel, S.; Erkey, C. Controlled drug delivery through a novel PEG hydrogel encapsulated silica aerogel system. *J. Biomed. Mater. Res. A* **2012**, *100A*, 1307–1315.

37 Magryta, J. Effect of aerogel on the properties of acrylonitrile-butadiene rubber (NBR) vulcanizates. *Polimery* **2012**, *57*, 117–123.

38 Lay, M.; Azura, A.; Othman, N.; Tezuka, Y.; Chhorda, P. Effect of nanosilica fillers on the cure characteristics and mechanical properties of natural rubber composites. *Adv. Mat. Res.* **2012**, *626*, 818–822.

39 Guo, W.-J.; Liu, L.; Liu, F. Y.; Yu, W.-W.; Jia, L.; He, H. W.; Zhu, F. B.; Zheng, Q. Mechanical properties and mullins effect of ethylene propylene diene monomer vulcanizes reinforced with silica powders with different micropore structures. *Acta Polymerica Sinica* (in Chinese) **2023**, *54*, 1241–1252.

40 Song, Y. H.; Zeng, L. B.; Zheng, Q. Understanding the reinforcement and dissipation of natural rubber compounds filled with hybrid filler composed of carbon black and silica. *Chinese J. Polym. Sci.* **2017**, *35*, 1436–1446.

41 Liu, Y. B.; Li, L.; Wang, Q. Reinforcement of natural rubber with carbon black/nanoclay hybrid filler. *Plast. Rubber Compos.* **2013**, *39*, 370–376.

42 Hou, F.; Song, Y.; Zheng, Q. Payne effect of thermo-oxidatively aged isoprene rubber vulcanizates. *Polymer* **2020**, *195*, 122432.

43 Štandeker, S.; Novak, Z.; Knez, Ž. Adsorption of toxic organic compounds from water with hydrophobic silica aerogels. *J. Colloid Interface Sci.* **2007**, *310*, 362–368.

44 Julve, D.; Ramos, J.; Pérez, J.; Menéndez, M. Analysis of mercury porosimetry curves of precipitated silica, as an example of compressible porous solids. *J. Non-Crystalline Solids* **2011**, *357*, 1319–1327.

45 Khang, T. H.; Ariff, Z. M. Vulcanization kinetics study of natural rubber compounds having different formulation variables. *J. Therm. Anal. Calorim.* **2011**, *109*, 1545–1553.

46 Yang, S. Y.; Jia, Z. X.; Liu, L.; Fu, W. W.; Jia, D. M.; Luo, Y. F. Insight into vulcanization mechanism of novel binary accelerators for natural rubber. *Chinese J. Polym. Sci.* **2014**, *32*, 1077–1085.

47 Yang, C.; Luo, Y.; Peng, Z.; Xu, K.; Zhong, J. Comparison effects of lanthanum stearate and antioxidants in epoxidized natural rubber. *J. Rare Earths* **2015**, *33*, 1236–1240.

48 Tokoro, T. In *Effects of temperature and surface roughness on the evaluation of hydrophobic properties of silicone rubber*, 2016 IEEE Conference on Electrical Insulation and Dielectric Phenomena (CEIDP), IEEE: **2016**; pp. 814–817.

49 Estaji, S.; Paydayesh, A.; Mousavi, S. R.; Khonakdar, H. A.; Abiyati, M. M. Polycarbonate/poly(methyl methacrylate)/silica aerogel blend composites for advanced transparent thermal insulations: mechanical, thermal, and optical studies. *Polym. Compos.* **2021**, *42*, 5323–5334.

50 Floess, J. K.; Field, R.; Rouanet, S. The use of vinyl functional aerogels for reinforcement of silicone rubbers. *J. Non-Crystalline Solids* **2001**, *285*, 101–108.

51 Poh, B. T.; Te, C. S. Cure index and activation energy of vulcanization of natural rubber and epoxidized natural rubber vulcanized in the presence of antioxidants. *J. Appl. Polym. Sci.* **2000**, *77*, 3234–3238.

52 Sun, Y.; He, J.; Zhong, B.; Zhu, L.; Liu, F. A synthesized multifunctional rubber additive and its improvements on the curing and antioxidative properties of styrene-butadiene rubber/silica composites. *Polym. Degrad. Stabil.* **2019**, *170*, 108999.

53 Zhong, B.; Shi, Q.; Jia, Z.; Luo, Y.; Chen, Y.; Jia, D. Preparation of silica-supported 2-mercaptobenzimidazole and its antioxidative behavior in styrene-butadiene rubber. *Polym. Degrad. Stabil.* **2014**, *110*, 260–267.

54 Talma, A. G.; Datta, S.; Huntink, N. M.; Datta, R. N. Rubber vulcanizates degradation and stabilization. *Rubber Chem. Technol.* **2007**, *80*, 436–480.

55 Smith, L. M.; Aitken, H. M.; Coote, M. L. The fate of the peroxyl radical in autoxidation: how does polymer degradation really occur. *Acc. Chem. Res.* **2018**, *51*, 2006–2013.

56 Wang, X.; Yang, K.; Zong, C.; Zhang, P. The evolution of microstructure of Styrene-Isoprene-Butadiene Rubber during the thermal-oxidative aging process using *in-situ* FTIR way. *Polym. Degrad. Stabil.* **2021**, *188*, 109573.

57 Li, J.; Zhou, C.; Cao, D.; Liu, H. Synergistic effects of amine-containing antioxidants on the aging performances of ethylene propylene diene rubber. *ChemistrySelect* **2020**, *5*, 4961–4966.

58 Wang, X.; Yang, K.; Zhang, P. Evaluation of the aging coefficient and the aging lifetime of carbon black-filled styrene-isoprene-butadiene rubber after thermal-oxidative aging. *Compos. Sci. Technol.* **2022**, *220*, 109258.

59 Mostafa, A.; Abouel-Kasem, A.; Bayoumi, M. R.; El-Sebaie, M. G. The influence of CB loading on thermal aging resistance of SBR and NBR rubber compounds under different aging temperature. *Mater. Des.* **2009**, *30*, 791–795.

60 Ha-Anh, T.; Vu-Khanh, T. Prediction of mechanical properties of polychloroprene during thermo-oxidative aging. *Polym. Test.* **2005**, *24*, 775–780.

61 Carli, L. N.; Bianchi, O.; Mauler, R. S.; Crespo, J. S. Accelerated aging of elastomeric composites with vulcanized ground scraps. *J. Appl. Polym. Sci.* **2012**, *123*, 280–285.

62 Tang, M.; Xing, W.; Wu, J.; Huang, G.; Xiang, K.; Guo, L.; Li, G. Graphene as a prominent antioxidant for diolefin elastomers. *J. Mater. Chem. A* **2015**, *3*, 5942–5948.

63 Bandzierz, K.; Reuvekamp, L.; Dryzek, J.; Dierkes, W.; Blume, A.; Bielinski, D. Influence of network structure on glass transition temperature of elastomers. *Materials* **2016**, *9*, 607.

64 Bellas, R.; Díez, J.; Rico, M.; Barral, L.; Ramírez, C.; Montero, B. Accelerated ageing of styrene-butadiene rubber nanocomposites stabilized by phenolic antioxidant. *Polym. Compos.* **2014**, *35*, 334–343.

65 Xiang, K.; Wu, S.; Huang, G.; Zheng, J.; Huang, J.; Li, G. Relaxation behavior and time-temperature superposition (TTS) profiles of thermally aged styrene-butadiene rubber (SBR). *Macromol. Res.* **2014**, *22*, 820–825.

https://doi.org/10.1007/s10118-024-3125-5